

# Effective Dynamic Properties and Multi-Resonant Design of Acoustic Metamaterials

R. Zhu

G. L. Huang

e-mail: glhuang@ualr.edu

Department of Systems Engineering,  
University of Arkansas at Little Rock,  
Little Rock, AR 72204

G. K. Hu

School of Aerospace Engineering,  
Beijing Institute of Technology,  
Beijing, China, 100081

*In the study, a retrieval approach is extended to determine the effective dynamic properties of a finite multilayered acoustic metamaterial based on the theoretical reflection and transmission analysis. The accuracy of the method is verified through a comparison of wave dispersion curve predictions from the homogeneous effective medium and the exact solution. A multiresonant design is then suggested for the desirable multiple wave band gaps by using a finite acoustic metamaterial slab. Finally, the band gap behavior and kinetic energy transfer mechanism in a multilayered composite with a periodic microstructure are studied to demonstrate the difference between the Bragg scattering mechanism and the locally resonant mechanism. [DOI: 10.1115/1.4005825]*

*Keywords:* acoustic metamaterials, negative effective mass density, band gaps, local resonance

## 1 Introduction

The ability of an acoustic bandgap material or a phononic crystal with a periodic arrangement of different phase inclusions to control wave propagation in certain frequency ranges has been the subject of intense investigation in recent years because of their novel physical properties and many potential applications [1–3]. Bragg-scattering-induced band gaps in phononic crystals exist when their mass density and bulk modulus are spatially modulated [4–6]. However, the band gaps induced by the Bragg scattering require the propagating wavelength to be on the order of the lattice (microstructure) constant. Limited by this requirement, large engineering structures are needed for environmental low-frequency sound and vibration shielding. One solution was first provided by Liu et al. [7] by periodically adding locally resonant microstructures (polymer-coated lead spheres) into the matrix material. The resulting internal resonance creates a low-frequency band gap in which the characteristic length of the microstructure is much smaller than the acoustic wavelength [8]. Subsequently, wave propagation in acoustic metamaterials and their unique properties have been explored intensively [9–13]. Various novel concepts were successfully demonstrated, such as the realization of acoustic metamaterials with a negative index of refraction [14], super environmental acoustic absorbers [15], the synthesis of acoustic metamaterials that enable wave focusing [16], acoustic metamaterials waveguides [17], acoustic metamaterials cloaking [18], subwavelength channels [19], acoustic superlenses [20], and active acoustic metamaterials [21]. One of the most fundamental issues related to the design of the acoustic metamaterials is to understand the wave propagation difference between the Bragg scattering and the local resonance mechanisms.

The essential features of phononic crystals and acoustic metamaterials can be captured by the one-dimensional (1D) multilayered medium [22–24], because the 1D medium provides an excellent platform for the rigorous analysis of the fundamental dynamic properties related to periodically heterogeneous materials and structures. The propagation of longitudinal and transverse elastic waves in an infinite periodically layered system was investigated by Wang et al. [22]. The system was constructed by inserting thin layers of soft rubber into stiff matrix layers to form the locally resonant structures. Zhao et al. [23] have theoretically and

experimentally studied the transmission peaks in the gap region of a specifically configured 1D phononic crystal. An experimental demonstration of an omnidirectional band gap for a longitudinal wave impinging on a finite multilayer of two elastic materials has been reported [25]. From a practical point of view, it is important to examine the dynamic properties of a finite periodic layered structure to interpret the observed physical phenomena. A transfer matrix formulation was used to derive a frequency-dependent function that describes the transmission of an incident harmonic wave from one end of a finite structure to the receiving end (Day et al. [26], Cao and Qi [27], Hussein et al. [28]).

For 1D acoustic metamaterials, dynamic effective parameters are appropriate since the unit cell is sub-wavelength size at the resonant frequency [29]. For example, the unusual low-frequency band gap can be attributed to the effective negative mass, which is defined as the out-of-phase motion between the resonant unit and the matrix material [8]. There is also a growing interest in studying the anisotropic mass density in the metamaterial community. Based on Schoenberg and Sen's work [30], Cheng et al. [31] designed an acoustic cloak with a concentric alternating layered structure with homogeneous isotropic materials on the basis of the effective medium theory. Torrent and Sánchez-Dehesa [32] experimentally demonstrated an acoustic metamaterial with anisotropic mass density, which is made of two fluidlike materials with different mass densities. Several homogenization methods have been developed to model infinite metamaterials with simple microstructure geometries as effective homogeneous media, of which the effective parameters, such as the effective mass density and modulus, were computed based on the long-wavelength limit [24,33,34]. However, there is a great demand to develop an efficient homogenization method for the finite metamaterials with complex microstructures, especially for the cases when the number of the unit cells is not large enough. For the electromagnetic metamaterials with finite lengths, their effective permittivity and permeability were determined by obtaining the effective refractive index and impedance independently from the experimentally measured reflection and transmission coefficients [35]. With the correct selection of the sign of the effective impedance  $z$  and the branch of the real part of the refractive index  $n$ , an improved method was suggested to retrieve the effective constitutive parameters of finite electromagnetic metamaterials from the measurement of  $S$  parameters [36]. For acoustic metamaterials, a retrieval method to obtain their effective properties from experimentally measured reflection and transmission coefficients was discussed; details of this method include the boundary position location of the metamaterials and the sign selections of the refractive index  $n$

Contributed by the Noise Control and Acoustics Division of ASME for publication in the JOURNAL OF VIBRATION AND ACOUSTICS. Manuscript received September 17, 2010; final manuscript received September 29, 2011; published online April 23, 2012. Assoc. Editor: Liang-Wu Cai.

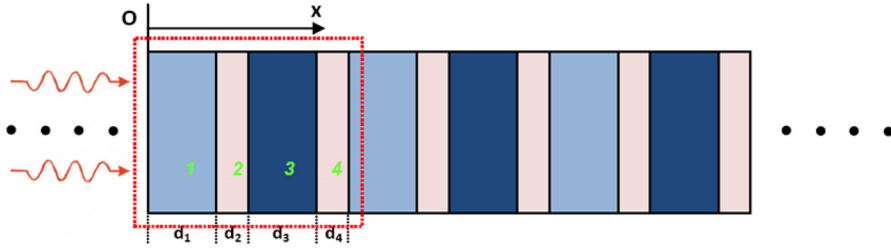


**Fig. 1 Longitudinal wave propagation in the infinite four-layered elastic medium**

and impedance  $z$  [37]. The method was also used to design non-resonant acoustic metamaterials made of periodic arrangements of highly subwavelength unit cells composed of one or more inclusions embedded in a fluid [38]. In this study, the improved method proposed by Chen et al. [36] will be adopted to determine dynamic effective properties of the finite acoustic metamaterial.

In this paper, a modified retrieval method is proposed to predict the effective dynamic properties of the finite 1D acoustic metamaterial based on the theoretical reflection and transmission analysis. A very good agreement of the dispersion curves predicted from the homogeneous effective medium and the exact solution shows the accuracy of the retrieval method. Based on the obtained effective dynamic properties, a multi-resonant design of the finite acoustic metamaterial is suggested and analyzed. Finally, a comprehensive study is conducted to show the difference between the Bragg scattering mechanism and the locally resonant mechanism through the wave propagation analysis in the 1D multilayered medium.

## 2 Dynamic Effective Properties of the Finite 1D Acoustic Metamaterial

In this section, the 1D finite acoustic metamaterial is constructed from the multilayered medium, as shown in Fig. 1. In the

figure, the four-layered elastic medium is constructed of layers with different thicknesses and material properties. In the figure,  $j$  ( $j=1, 2, 3$ , and  $4$ ) represents the number of the layer in the unit cell. Layer 3 contains the stiffest material, layer 1 contains the second stiffest material, layers 2 and 4 contain the same very soft material. The elastic Lamé constants, the mass density, and the thickness of the layer  $j$  are denoted as  $\lambda_j$ ,  $\mu_j$ ,  $\rho_j$ , and  $d_j$ , respectively. The total length of the unit cell is defined as  $a = d_1 + d_2 + d_3 + d_4$ .

The effective dynamic properties of the 1D finite acoustic metamaterial will be retrieved from the theoretical reflection and transmission analysis. The finite multilayered structure considered is assumed to be immersed in an infinite homogeneous elastic medium which has the same property as that of layer 1 in the unit cell. To simplify the problem, only the longitudinal wave propagation will be demonstrated. It should be mentioned that similar physical phenomena can also be obtained for the transverse and out-of-plane waves. We define a vector  $\mathbf{a}_j = [A_j^+ \ A_j^-]$ , where  $A_j^+$  and  $A_j^-$  are wave amplitude constants in layer  $j$ . Then, a transfer matrix between  $\mathbf{a}_j$  and  $\mathbf{a}_{j+1}$  can be defined as

$$\mathbf{a}_j = \bar{\mathbf{T}}_{j,p} \mathbf{a}_{j+1} \quad (1)$$

with

$$\bar{\mathbf{T}}_{j,p} = \frac{1}{2Z_j} \begin{bmatrix} (Z_j + Z_{j+1}) \exp(i(k_{j+1} - k_j)x_{j,p}^R) & (Z_j - Z_{j+1}) \exp(-i(k_{j+1} + k_j)x_{j,p}^R) \\ (Z_j - Z_{j+1}) \exp(i(k_{j+1} + k_j)x_{j,p}^R) & (Z_j + Z_{j+1}) \exp(-i(k_{j+1} - k_j)x_{j,p}^R) \end{bmatrix} \quad (2)$$

where  $\bar{\mathbf{T}}_{j,p}$  is the transfer matrix, subscript  $p$  represents the  $p$ th unit cell in the finite multilayered structure and  $x_{j,p}^R$  is the position of the right boundary of the layer  $j$  in the  $p$ th unit cell, and  $Z_j$  is the impedance of layer  $j$ . For the finite multilayered medium with  $N_{\text{cell}}$  unit cells, we have

$$\bar{\mathbf{T}}_{N_{\text{cell}}} = \prod_{p=1}^{N_{\text{cell}}} (\bar{\mathbf{T}}_{1,p} \cdot \bar{\mathbf{T}}_{2,p} \cdot \bar{\mathbf{T}}_{3,p} \cdot \bar{\mathbf{T}}_{4,p}) \quad (3)$$

where

$$\begin{aligned} \bar{\mathbf{T}}_{1,p} &= \frac{1}{2Z_1} \begin{bmatrix} (Z_1 + Z_2)e^{i(k_2 - k_1)[d_1 + a(p-1)]} & (Z_1 - Z_2)e^{-i(k_2 + k_1)[d_1 + a(p-1)]} \\ (Z_1 - Z_2)e^{i(k_2 + k_1)[d_1 + a(p-1)]} & (Z_1 + Z_2)e^{-i(k_2 - k_1)[d_1 + a(p-1)]} \end{bmatrix} \\ \bar{\mathbf{T}}_{2,p} &= \frac{1}{2Z_2} \begin{bmatrix} (Z_2 + Z_3)e^{i(k_3 - k_2)[d_1 + d_2 + a(p-1)]} & (Z_2 - Z_3)e^{-i(k_3 + k_2)[d_1 + d_2 + a(p-1)]} \\ (Z_2 - Z_3)e^{i(k_3 + k_2)[d_1 + d_2 + a(p-1)]} & (Z_2 + Z_3)e^{-i(k_3 - k_2)[d_1 + d_2 + a(p-1)]} \end{bmatrix} \\ \bar{\mathbf{T}}_{3,p} &= \frac{1}{2Z_3} \begin{bmatrix} (Z_3 + Z_4)e^{i(k_4 - k_3)[d_1 + d_2 + d_3 + a(p-1)]} & (Z_3 - Z_4)e^{-i(k_4 + k_3)[d_1 + d_2 + d_3 + a(p-1)]} \\ (Z_3 - Z_4)e^{i(k_4 + k_3)[d_1 + d_2 + d_3 + a(p-1)]} & (Z_3 + Z_4)e^{-i(k_4 - k_3)[d_1 + d_2 + d_3 + a(p-1)]} \end{bmatrix} \\ \bar{\mathbf{T}}_{4,p} &= \frac{1}{2Z_4} \begin{bmatrix} (Z_4 + Z_1)e^{i(k_1 - k_4)ap} & (Z_4 - Z_1)e^{-i(k_4 + k_1)ap} \\ (Z_4 - Z_1)e^{i(k_4 + k_1)ap} & (Z_4 + Z_1)e^{-i(k_1 - k_4)ap} \end{bmatrix} \end{aligned}$$

Thus, wave propagation in the finite structure can be described as

$$\mathbf{a}_1 = \bar{\mathbf{T}}_{N_{\text{cell}}} \mathbf{a}_{N_{\text{cell}}+1} \quad (4)$$

In Eq. (4),  $\mathbf{a}_{N_{\text{cell}}+1}$  is the vector describing the dynamic response in the matrix medium in which the finite structure is immersed. Based upon Eq. (4), the transmission coefficient  $T_c$  and reflection coefficient  $R_c$  in the structure can be obtained as [39]

$$T_c = \frac{1}{\bar{\mathbf{T}}_{N_{\text{cell}}}(1, 1)} \exp(iN_{\text{cell}}ka) \quad (5)$$

$$R_c = \frac{\bar{\mathbf{T}}_{N_{\text{cell}}}(2, 1)}{\bar{\mathbf{T}}_{N_{\text{cell}}}(1, 1)} \quad (6)$$

Once the transmission and reflection coefficients are obtained, the effective impedance  $Z$  and the refractive index  $n$  can be calculated as [36]

$$n = \frac{\pm \cos^{-1}\left(\frac{1}{2T_c} [1 - (R_c^2 - T_c^2)]\right)}{ka} + \frac{2\pi m}{ka} \quad (7)$$

$$Z = \pm \sqrt{\frac{(1 + R_c)^2 - T_c^2}{(1 - R_c)^2 - T_c^2}} \quad (8)$$

where  $m$  is the branch number of the  $\cos^{-1}$  function. To obtain the effective impedance  $Z$  and refractive index  $n$ , the signs of  $Z$  and  $n$  along with the branch number 'm' of the  $\cos^{-1}$  function should be uniquely determined. In the study, these issues are solved by imposing additional constraints on the acoustic metamaterial properties and using the conditions that  $Z$  and  $n$  are continuous functions of frequency. In order to do this, Eqs. (7) and (8) can be rewritten as [37]

$$Z = \frac{r}{1 - 2R_c + R_c^2 - T_c^2} \quad (9)$$

$$n = \frac{-i \log x + 2\pi m}{ka} \quad (10)$$

where  $r = \mp \sqrt{(R_c^2 - T_c^2 - 1)^2 - 4T_c^2}$  and  $x = (1 - R_c^2 - T_c^2 - r)/2T_c$ . Since the acoustic metamaterial under consideration is a passive medium, the real part of the impedance  $Z$  should be positive [35–37]

$$Z' \geq 0 \quad (11)$$

where  $(\cdot)'$  denotes the real part operator. Based on Eq. (11), the signs in Eqs. (7) and (8) can be uniquely determined. However, when the thickness of the finite acoustic metamaterial is large, the value of  $Z'$  could be very small. In this situation, only using  $Z' \geq 0$  may cause incorrect combinations of the signs of  $Z$  and  $n$ . A positive imaginary wave velocity component is required to restrict the imaginary part of  $n$  to a negative value [37]

$$n'' \leq 0 \quad (12)$$

where  $(\cdot)''$  denotes the imaginary part operator. In summary, a procedure for the selection of  $Z$  and  $n$  is suggested as follows: (i) for  $|Z'| \geq A^0$  with  $A^0$  being a positive number,  $Z' \geq 0$  is selected; (ii) for  $|Z'| \leq A^0$ ,  $n'' \leq 0$  is selected [36]. For the determination of the branch of  $n'$ , the proper branch number  $m$  can be determined by an iterative method using the mathematical continuity of the parameters.

### 3 Numerical Results and Discussion

Let us now consider a four-layered medium as the 1D counterpart of the three-dimensional ternary system which consists of

**Table 1 Material properties for two multi-layered media**

Types of multi-layered media	Material properties					
	$\rho_3/\rho_1^a$	$\rho_3/\rho_2^a$	$\rho_3/\rho_4^a$	$E_3/E_1^a$	$E_3/E_2^a$	$E_3/E_4^a$
Layered medium I	10:1	10:1	10:1	10:1	10:1	10:1
Layered medium II	10:1	10:1	10:1	10:1	10 <sup>5</sup> :1	10 <sup>5</sup> :1

<sup>a</sup>Here,  $\rho_3$  is 11160 kg/m<sup>3</sup> and  $E_3$  is 40.8 GPa.

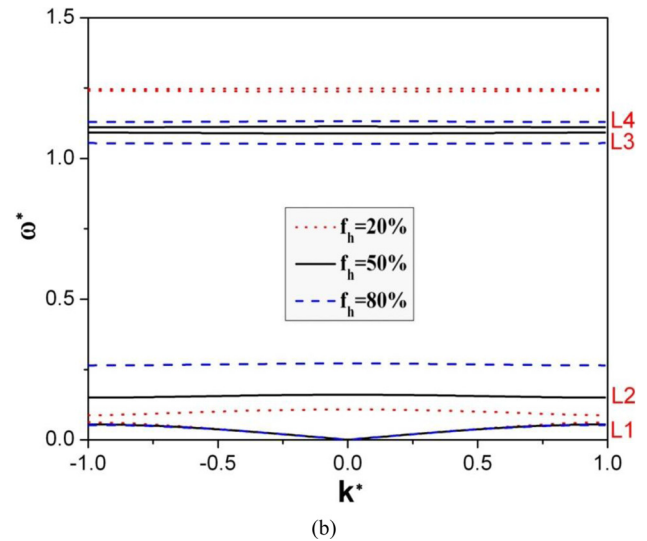
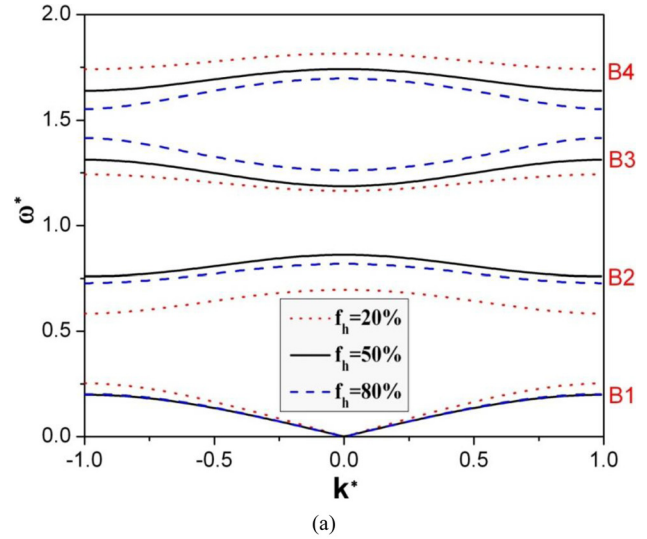


**Fig. 2 Dispersion curves of the two four-layered elastic media with different filling fractions: (a) layered medium I (the Bragg scattering mechanism), and (b) layered medium II (the locally resonant mechanism)**

coated spheres immersed in a matrix medium in a cubic array, as shown in Fig. 1. Two four-layered media with different material mismatches are selected in Table 1.

In this study, only the longitudinal wave propagation normal to the layer direction will be studied. Figure 2 shows the dispersion curves of the two four-layered media with the different material mismatches listed in Table 1 and different filling fractions  $f_h$  with  $f_h = (d_1 + d_3 + d_4)/a \times 100\%$ , respectively. In the figure, the normalized wave frequency is  $\omega^* = \omega a / 2\pi c_{l,ave}$  and the normalized wave number is  $k^* = ka / \pi$  with  $c_{l,ave} = a / (d_1 c_{l,1}^{-1} + d_2 c_{l,2}^{-1} + d_3 c_{l,3}^{-1} + d_4 c_{l,4}^{-1})$  and  $c_{l,j}$  being the longitudinal wave velocity in the  $j$ th layer.

A numerical analysis is conducted in the section. Specifically, the effective dynamic properties of the 1D finite acoustic metamaterial, which is layered medium II with  $f_h = 50\%$  in Table 1, will be calculated based on the discussion in Sec. 2. The accuracy of the method is verified by comparing the dispersion curves predicted from the homogeneous effective medium and the exact solution. A multiresonant design of the finite acoustic metamaterial will be suggested for the desired multiple band gaps. Finally, the difference between the Bragg scattering mechanism and the locally resonant mechanism will be demonstrated by kinetic energy distribution in the multilayered medium.

**3.1 Effective Dynamic Properties of the 1D Acoustic Metamaterial.** In this subsection, a locally resonant layered medium, which is a good candidate as a 1D acoustic metamaterial, is studied by introducing a resonant unit into the building block. The layered medium II with a filling fraction of  $f_h = 50\%$  is selected. A modified retrieval method is used to obtain the effective material properties of the 1D acoustic metamaterial. According to Sec. 2, the effective dynamic properties of the acoustic metamaterial can be obtained as

$$E_{eff} = Zc \quad (13)$$

$$\rho_{eff} = \frac{Z}{c} \quad (14)$$

where  $c = c_{l,1}/n$ , and  $Z$  and  $n$  are determined by the theoretically obtained transmission and reflection coefficients.

Figure 3 shows the normalized effective mass density and effective modulus based on Eqs. (13) and (14) over a large band of frequencies for the finite acoustic metamaterials with three, five, and eight unit cells, respectively. The normalized effective modulus and mass density are defined as  $E_{eff}^* = E_{eff}/E_{eff}^0$  and  $\rho_{eff}^* = \rho_{eff}/\rho_{eff}^0$ , respectively, where  $E_{eff}^0 = 4.078$  MPa and  $\rho_{eff}^0 = 6380$  kg/m<sup>3</sup> are the effective static Young's modulus and mass density, which are calculated based on the volume average of the component material properties. In Fig. 3(a), it is shown that at the low frequency limit, the effective mass density can be recovered to the volume-averaged mass density (VAMD) for the current layered medium with the matrix layer being a solid. However, if the matrix is a fluid, inertia is important, and so one might not expect to obtain the VAMD at the low frequency limit [40]. More than two decades ago, Berryman [41,42] derived a different effective mass density expression for the prediction of (fluid matrix-solid or fluid matrix-fluid) composite wave properties in the long wavelength limit, based on the average T-matrix approach. The physical reason for this difference was recently explained by Mei et al. [43], Torrent et al. [44], and Martin et al. [40].

It can be seen that the current method is not sensitive to the thickness of the finite acoustic metamaterial slab. The extracted effective dynamic material parameters with different unit cells are virtually identical, which shows that the acoustic metamaterial slab with a few unit cells can be used for the characterization of its effective dynamic properties. In Fig. 3(a), it can be observed that the real part of the effective mass density is negative in the normalized frequency range  $\omega^* = (0.05, 0.16)$ , which is very close to the first band gap shown in Fig. 2(b). The negative value of the effective mass density can be understood as the stiffest layer A moving out-of-phase with the driving field at resonance. As shown in Fig. 3(b), the effective elastic modulus is always positive in the first band gap. Although both the effective modulus and the effective mass density have imaginary parts inside the resonant gap, this fact does not indicate any absorption or gain, since all the constituent blocks of the model are conventional elastic materials. To validate the current method, Fig. 4 shows the comparison between the dispersion curves of the acoustic metamaterial predicted by using the exact solution and the homogeneous medium with the obtained effective parameters. A very good

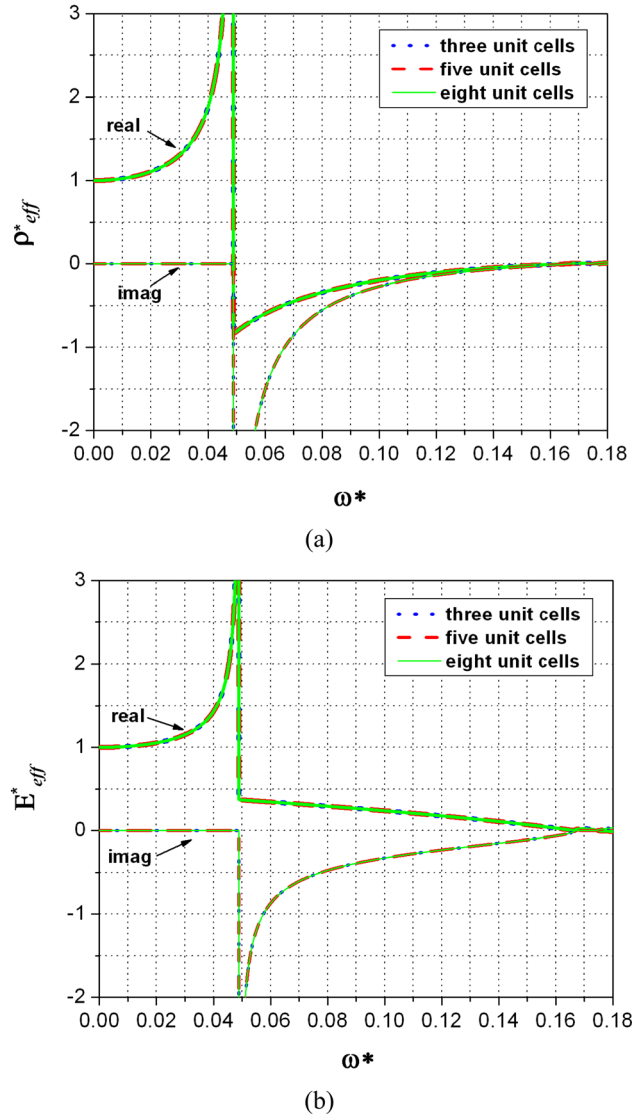


Fig. 3 Effective material properties of the finite 1D acoustic metamaterials with different lengths: (a) normalized effective mass density, and (b) normalized effective elastic modulus

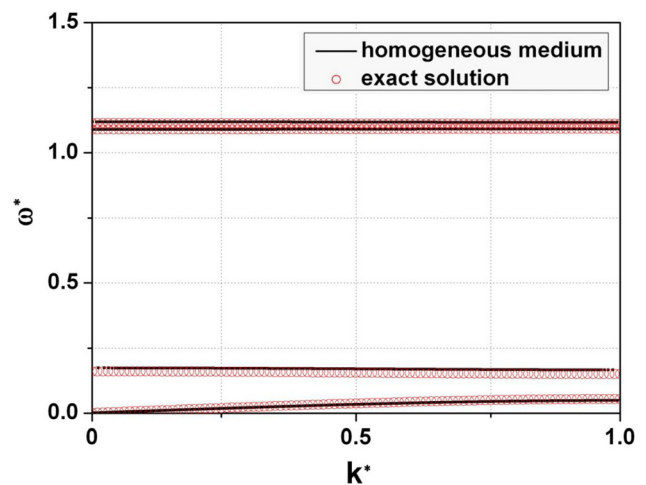


Fig. 4 Comparison of the dispersion curves predicted by using the homogeneous medium with obtained effective parameters and the exact solution

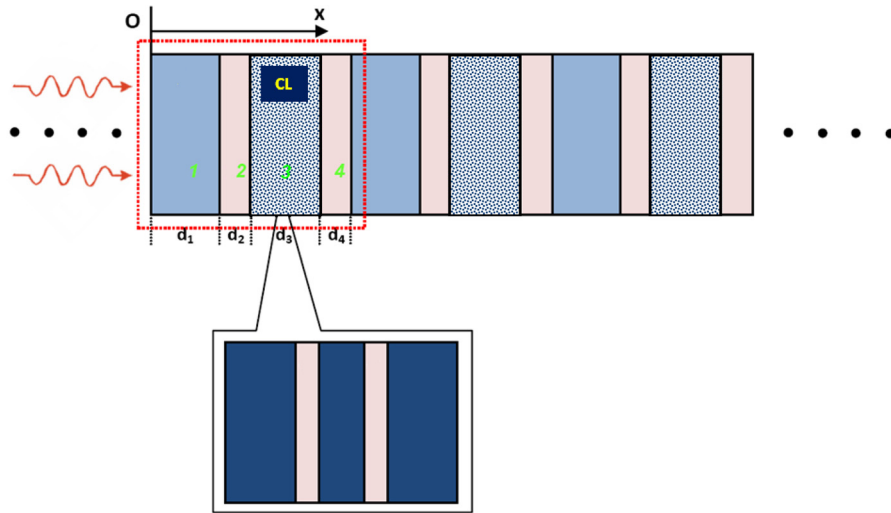


Fig. 5 A proposed layer-in-layer acoustic metamaterial

agreement is observed even for high-order wave modes, which indicates the accuracy of the retrieval method for the prediction of the effective dynamic parameters of the acoustic metamaterial. It should be mentioned that the obtained dynamic properties are only for the direction perpendicular to the layered medium. However, in a manner similar to other periodic multilayer structures, the dynamic properties of the layered medium are anisotropic. To obtain the dynamic properties of the layered medium along other directions, the wave propagation in the finite acoustic metamaterial slab along other directions should be investigated.

**3.2 Multiresonant Design of the Acoustic Metamaterial.** In general, the aforementioned layered media have only one low frequency band gap and may not be suitable for some device applications which need multiple band gaps, especially in the low frequency ranges. In order to design multiple band gaps at the desired frequency regime, a multiresonant layer-in-layer system is needed. In this subsection, multiple wave band gaps in low frequency ranges produced by a layer-in-layer system

are investigated and the band structure is designed and controlled by using different microstructure combinations. Attention is focused on the roles played by the layer-in-layer system. A multiresonant design of the layer-in-layer system is proposed. In comparison with the original unit cell, the stiffest layer is replaced by a composite layer (CL) in the new unit cell to generate multiple band gaps as shown in Fig. 5. For simplicity, three layers made of the stiffest material and two layers made of the softest material are selected to build the composite layer. The detailed structure of the composite layer (CL) can be found in the magnified area of Fig. 5. The three-dimensional counterpart of this layer-in-layer system is the triple-coated spherical inclusions embedded in the matrix medium. The center stiff layer in the composite layer can be regarded as the core and the other stiff layers function as the shell when the frequency is low. The length ratio between the core and shell layers in the composite layer is defined as  $r_p = L_{core}/L_{shell}$ , where  $L_{core}$  is the length of the core layer and  $L_{shell}$  is the total length of the two shell stiff layers.

Based on the retrieval method, the effective mass density and effective elastic modulus of the layer-in-layer system can be

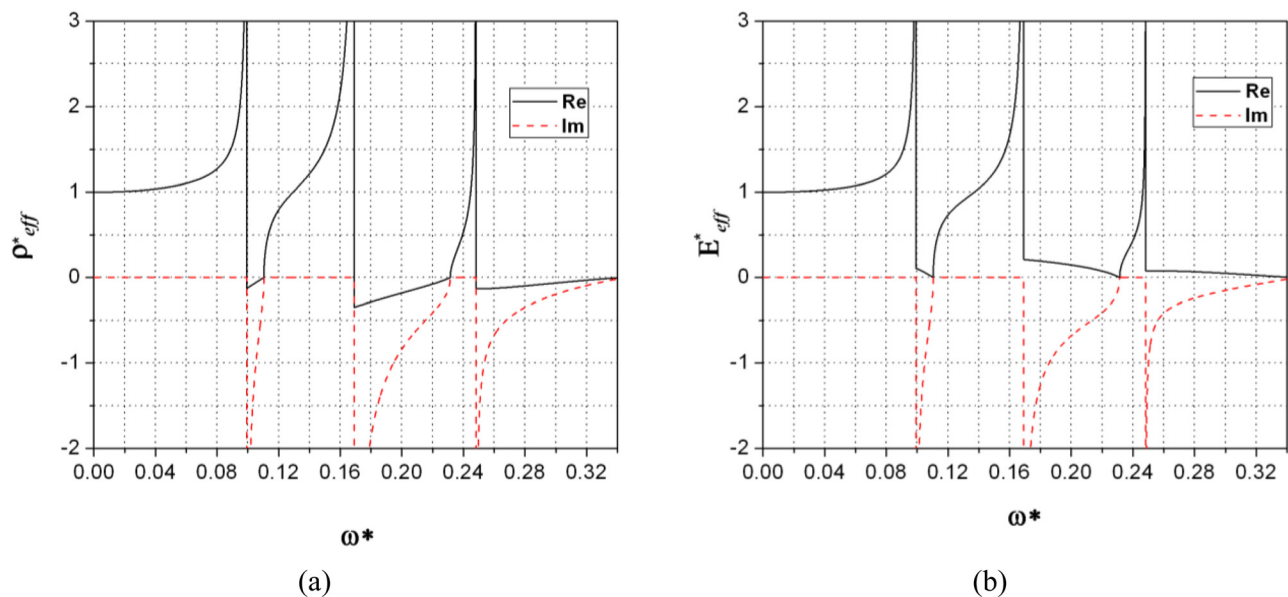
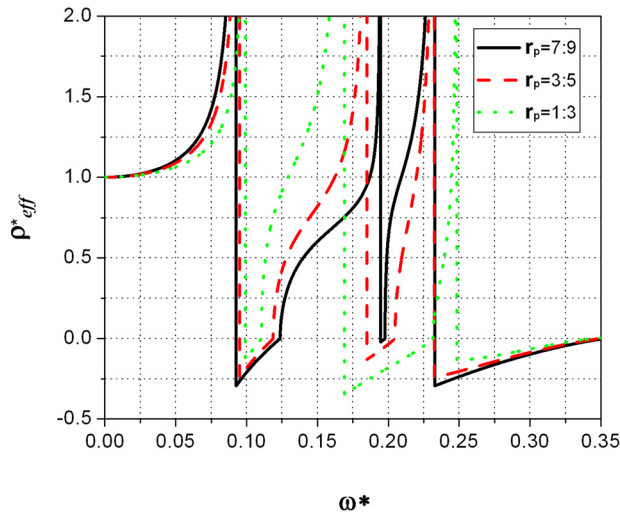


Fig. 6 Effective material properties of the layer-in-layer metamaterial with  $r_p = 1:3$ : (a) normalized effective mass density, and (b) normalized effective elastic modulus



**Fig. 7 Effective mass densities of the layer-in-layer metamaterials with different core-shell ratios  $r_p$  in the composite layers**

estimated. Figures 6(a) and 6(b) show the effective mass density and effective modulus in the layer-in-layer system when  $r_p = 1 : 3$ , respectively. It is demonstrated that several band gaps are formed by using the proposed layer-in-layer system. As shown in Fig. 6(a), compared with the first band gap  $\omega^* = (0.05, 0.16)$  in the original layered medium II, three new small band gaps  $\omega^* = (0.099, 0.11)$ ,  $\omega^* = (0.169, 0.231)$ , and  $\omega^* = (0.248, 0.344)$  in a similar frequency range are created. Negative effective mass densities can be found in all three new band gaps. Alternatively, two new pass bands are generated in the ranges  $\omega^* = (0.11, 0.169)$  and  $\omega^* = (0.231, 0.248)$  by using the layer-in-layer system. As expected, the effective mass densities inside the two pass bands are positive. In Fig. 6(b), the effective elastic modulus of the new acoustic metamaterial is always positive.

It should be noted that the new pass bands can also be designed and controlled by changing the microstructures of the layer-in-layer system. Figure 7 shows the effective mass densities of the layer-in-layer system with various length ratios of the core and shell layers. From the figure, it can be found that the two new pass bands are changed to  $\omega^* = (0.1187, 0.1848)$  and  $\omega^* = (0.2047, 0.2326)$ , respectively, when the length ratio is  $r_p = 3:5$ . When  $r_p = 7:9$ , the two new pass bands are observed in  $\omega^* = (0.1236, 0.1975)$  and  $\omega^* = (0.1977, 0.2326)$ .

**3.3 The Bragg Scattering Mechanism and the Locally Resonant Mechanism.** It is well known that band gaps in the multilayered medium are caused by either the Bragg scattering mechanism or the locally resonant mechanism due to the different material mismatches. In this subsection, the difference between the Bragg scattering mechanism and the locally resonant mechanism will be demonstrated. From Figs. 2(a) and 2(b), it is noticed that the band edge of the first band gap (denoted as B1) is sensitive to the filling fraction of the layered medium I, which is associated with the Bragg scattering [22]. The largest band gap width is observed at the middle range of the filling fraction ( $f_h = 50\%$ ) for the Bragg scattering mechanism. However, for the layered medium II, the band edge of the first band gap (denoted as L1), which is caused by the local resonance, is not sensitive to the filling fraction. The band gap width increases with the increase of the filling fraction for the locally resonant mechanism. Additionally, the central frequency of the first band gap caused by the locally resonant mechanism is much lower than that caused by the Bragg scattering mechanism.

To further demonstrate the difference between the Bragg scattering mechanism and the locally resonant mechanism, kinetic

**Table 2 Kinetic energy distribution ratio  $R_j$  in each layer**

Types of multi-layered media	Band edges	$R_1(\%)$	$R_2(\%)$	$R_3(\%)$	$R_4(\%)$
Layered medium I (Bragg scattering)	B1	2.72	0.97	95.34	0.97
	B2	89.795	0.973	8.259	0.973
	B3	13.112	1.365	84.159	1.365
	B4	90.324	1.699	6.279	1.699
Layered medium II (local resonance)	L1	0	0.414	99.172	0.414
	L2	93.604	3.198	0	3.198
	L3	0	49.748	0.504	49.748
	L4	0.894	49.553	0	49.553

energy distributions in the two multilayered systems are studied at the band edges. In the study, the viscosities in both systems are ignored, which means that the elastic wave energy cannot be dissipated. For elastic wave propagation, the velocity of the energy transport is represented by the group velocity, and the group velocity approaches zero when the wave frequencies approach the band edges, which are denoted as L1, L2, L3, and L4 and B1, B2, B3, and B4 in Fig. 2. This implies that the kinetic energy distribution in the system becomes stationary [45]. It is of interest to find the stored kinetic energy distribution in different layers of the layered medium. For the locally resonant mechanism, it is believed that the kinetic energy is mainly stored in the resonator at the band edge. For the Bragg scattering mechanism, the kinetic energy is distributed in each layer instead. To quantify the kinetic energy distribution in the multilayered system, the kinetic energy in each layer is defined as

$$KE_j = \int_{x_j^R}^{x_j^L} \frac{\rho_j}{2} \dot{u}^2(x, t) dx, \quad j = 1, 2, 3, 4 \quad (15)$$

where the subscript  $j$  represents the number of the layer in the unit cell, the superscripts  $L$  and  $R$  represent the left and right boundaries of layer  $j$ , respectively, and  $u$  represents the normalized displacement along the  $x$  direction in layer  $j$ , which is obtained from the solution of the eigenvalue problem of the system. Then, the kinetic energy distribution ratio  $R_j$  in each layer can be defined as

$$R_j = \frac{KE_j}{KE_{total}} \times 100\% \quad (16)$$

where  $KE_{total} = \sum_{j=1}^4 KE_j$  represents the total kinetic energy in the unit cell.

Table 2 lists the kinetic energy distribution ratio in each layer of the two multilayered media at the corresponding four lowest band edges with the filling fractions being 50%.

It can be found that almost all of the kinetic energy concentrates in the resonator structure (total: 100%), which includes the major resonator and the connecting medium, in the layered medium II (local resonance). Specifically, as listed in Table 2, the resonator structure is represented by layers 2, 3, and 4 at the band edges L1 and L3; the resonator structure is represented by layers 4, 1, and 2 at the band edges L2 and L4. Compared with the kinetic energy distribution at band edge L1, the redistribution of the kinetic energy in layers 2, 3, and 4 at band edge L3 is due to the change of the major resonator from layer 3 to layers 2 and 4 in a higher-order resonant mode. A similar explanation holds for the cases at the band edges L2 and L4. However, every layer has nonzero kinetic energy in the layered medium I (Bragg scattering) for any frequencies at B1, B2, B3, and B4.

It is well known that material mismatch in the multilayered medium is an important parameter to change the wave propagation mechanism from the local resonance to the Bragg scattering, or the reverse. As an example, Fig. 8(a) shows the variation of the kinetic energy distribution ratio  $R_{2-3-4} = R_2 + R_3 + R_4$  in layers 2, 3, and 4 with different material mismatches and filling fractions  $f_h$

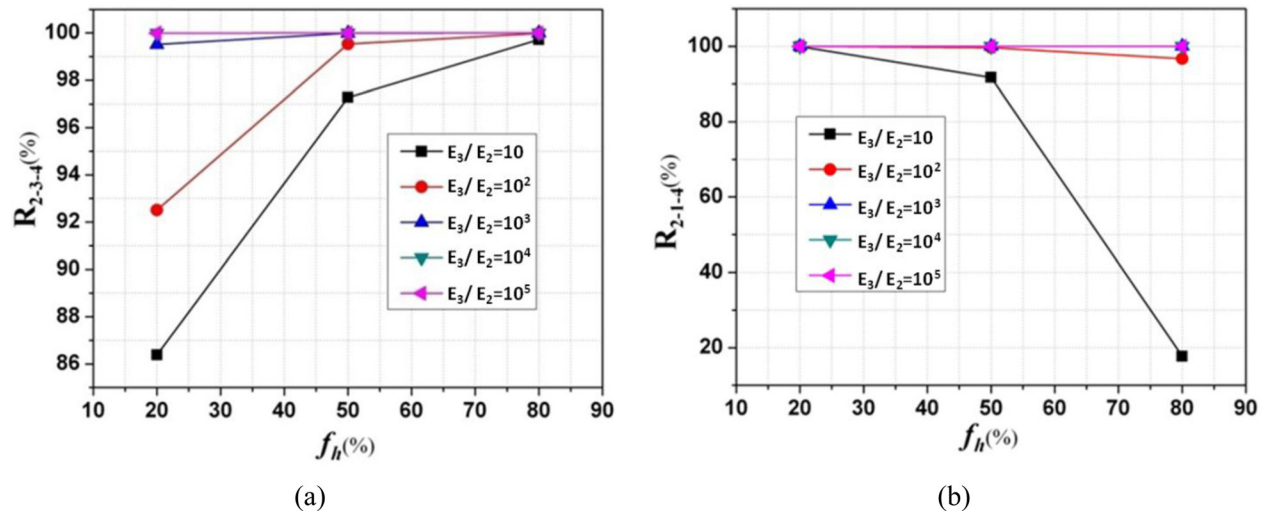


**Fig. 8** Kinetic energy distribution ratios of (a)  $R_{2-3-4}$  with different material mismatches and filling fractions  $f_h$  in the layered medium II at the corresponding first band edge frequency. (b)  $R_{2-1-4}$  with different material mismatches and filling fractions  $f_h$  in the layered medium II at the corresponding second band edge frequency.

in the multilayered media at the corresponding first band edge frequency. In the figure, the ratio  $E_3/E_2$  is used to represent the modulus mismatch between the material in layer 3 and the material in layer 2. It can be found that when the value of  $E_3/E_2$  approaches  $10^3$  or above, the kinetic energy distribution ratio  $R_{2-3-4}$  stays constant (around 100%) despite the changes in the filling fraction. It is expected because the total kinetic energy in the resonator structure is not sensitive to the size of the resonator structure based on the locally resonant mechanism. However, when the value of  $E_3/E_2$  is lower than  $10^3$ , the kinetic energy distribution ratio  $R_{2-3-4}$  increases with the increase of  $f_h$ . It is also understandable for the Bragg scattering mechanism because the kinetic energy distributed in each layer is sensitive to its size. An intermediate regime exists where the system properties are somewhere between the locally resonant mechanism and the Bragg scattering mechanism, and the assignment to either category would become somewhat arbitrary. Figure 8(b) shows the variation of the kinetic energy distribution ratio  $R_{2-1-4} = R_2 + R_1 + R_4$  in layers 2, 1, and 4 with different material mismatches and filling fractions  $f_h$  in the multilayered media at the corresponding second band edge frequency. A similar phenomenon can be observed to show the difference between the locally resonant mechanism and the Bragg scattering mechanism.

#### 4 Conclusion

In this paper, a modified retrieval method is extended to obtain the effective dynamic properties of the finite acoustic metamaterials based on the theoretical reflection and transmission analysis. The method is verified through the comparison of wave dispersion curve predictions from the homogeneous effective medium and the exact solution. Based on the obtained effective dynamic properties, a multiresonant design of the finite acoustic metamaterial is then proposed for the application of the multiple band gaps. Finally, the difference between the Bragg scattering mechanism and the locally resonant mechanism is demonstrated by analyzing the band structures and the kinetic energy distribution in the layered medium.

#### Acknowledgment

This research was partly supported by the Air Force Office of Scientific Research under Grant No. AF 9550-10-0061 with Program Manager Dr. Byung-Lip (Les) Lee and NSF Grant No. 1037569 and, in part, by the National Natural Science Foundation of China under Grant No. 10832002.

#### References

- [1] Martínez-Sala, R., Sancho, J., Sánchez, J. V., Gómez, V., Llinares, J., and Mesguer, F., 1995, "Sound Attenuation by Sculpture," *Nature (London)*, **378**, p. 241.
- [2] Huang, G. L. and Sun, C. T., 2010, "Band Gaps in a Multiresonator Acoustic Metamaterial," *ASME J. Vib. Acoust.*, **132**, p. 031003.
- [3] Milton, G. W. and Willis, J. R., 2007, "On Modification of Newton's Second Law and Linear Continuum Elastodynamics," *Proc. R. Soc. London, Ser. A*, **463**, p. 855.
- [4] Sigalas, M. M. and Economou, E. N., 1992, "Elastic and Acoustic Wave Band Structure," *J. Sound Vib.*, **158**, p. 377.
- [5] Kushwaha, M. S., Halevi, P., Dobrzynski, L., and Djafari-Rouhani, B., 1993, "Acoustic Band Structure of Periodic Elastic Composites," *Phys. Rev. Lett.*, **71**, p. 2022.
- [6] Montero de Espinosa, F. R., Jimenez, E., and Torres, M., 1998, "Ultrasonic Band Gap in a Periodic Two-dimensional Composite," *Phys. Rev. Lett.*, **80**, p. 1208.
- [7] Liu, Z. Y., Zhang, X. X., Mao, Y. W., Zhu, Y. Y., Yang, Z. Y., Chan, C. T., and Sheng, P., 2000, "Locally Resonant Sonic Materials," *Science*, **289**, p. 1734.
- [8] Sheng, P., Zhang, X. X., Liu, Z. Y., and Chan, C. T., 2003, "Locally Resonant Sonic Materials," *Physica B*, **338**, p. 201.
- [9] Zhou, X. M., Hu, G. K., and Lu, T. J., 2008, "Elastic Wave Transparency of a Solid Sphere Coated with Metamaterials," *Phys. Rev. B*, **77**, p. 024101.
- [10] Yao, S. S., Zhou, X. M., and Hu, G. K., 2008, "Experimental Study on Negative Effective Mass in a 1D Mass-Spring System," *New J. Phys.*, **10**, p. 043020.
- [11] Lee, S. H., Kim, C. K., Park, C. M., Seo, Y. M., Wang, Z. G., and Kim, C. K., 2009, "Acoustic Metamaterial with Negative Modulus," *J. Phys.: Condens. Matter*, **21**, p. 175704.
- [12] Lee, S. H., Park, C. M., Seo, Y. M., Wang, Z. G., and Kim, C. K., 2009, "Acoustic Metamaterial with Negative Density," *Phys. Lett. A*, **373**, p. 4464.
- [13] Huang, H. H., Sun, C. T., and Huang, G. L., 2009, "On the Negative Effective Mass Density in Acoustic Metamaterials," *Int. J. Eng. Sci.*, **47**, p. 610.
- [14] Li, J. and Chan, C. T., 2004, "Double-Negative Acoustic Metamaterial," *Phys. Rev. E*, **70**, p. 055602.
- [15] Pai, P. F., 2010, "Metamaterial-Based Broadband Elastic Wave Absorber," *J. Intell. Mater. Syst. Struct.*, **21**, p. 517.
- [16] Zhang, S. Yin, L. L., and Fang, N., 2009, "Focusing Ultrasound with an Acoustic Metamaterial Network," *Phys. Rev. Lett.*, **102**, p. 194301.
- [17] Torrent, D. and Sánchez-Dehesa, J., 2007, "Acoustic Metamaterials for New Two Dimensional Sonic Devices," *New J. Phys.*, **9**, p. 323.
- [18] Torrent, D. and Sánchez-Dehesa, J., 2008, "Acoustic Cloaking in Two Dimensions: A Feasible Approach," *New J. Phys.*, **10**, p. 063015.
- [19] Zhu, J., Christensen, J., Jung, J., Martín-Moreno, L., Yin, X., Fok, L., Zhang, X., and García-Vidal, F. J., 2011, "A Holey-Structured Metamaterial for Acoustic Deep-Subwavelength Imaging," *Nature Phys.*, **7**, p. 52.
- [20] Li, J., Fok, L., Yin, X. B., Bartal, G., and Zhang, X., 2009, "Experimental Demonstration of an Acoustic Magnifying Hyperlens," *Nature Mater.*, **8**, p. 931.
- [21] Baz, Amr. M., 2010, "An Active Acoustic Metamaterial With Tunable Effective Density," *ASME J. Vib. Acoust.*, **132**, p. 041011.
- [22] Wang, G., Yu, D. L., Wen, J. H., Liu, Y. Z., and Wen, X. S., 2004, "One-Dimensional Phononic Crystals with Locally Resonant Structures," *Phys. Lett. A*, **327**, p. 512.
- [23] Zhao, D., Wang, W., Liu, Z., Shi, J., and Wen, W., 2007, "Peculiar Transmission Property of Acoustic Waves in a One-Dimensional Layered Phononic Crystal," *Physica B*, **390**, pp. 159-166.
- [24] Nemat-Nasser, S., and Willis, J. R., 2011, "Homogenization of Periodic Elastic Composites and Locally Resonant Sonic Materials," *Phys. Rev. B*, **83**, p. 104103.

- [25] Manzanares-Martínez, B., Sánchez-Dehesa, J., Håkansson, A., Cervera, F., and Ramos-Mendieta, F., 2004, "Experimental Evidence of Omnidirectional Elastic Bandgap in Finite One-dimensional Phononic Systems," *Appl. Phys. Lett.*, **85**, p. 154.
- [26] Day, N. A., Zhu, C., and Kinra, V. K., 1994, "A Study of Dispersive Waves Propagation in Periodic Layered Composites," *Rev. Prog. Quant. Nondestruct. Eval.*, **13**, pp. 243–250.
- [27] Cao, W. W. and Qi, W. K., 1995, "Plane-Wave Propagation in Finite 2-2-Composites," *J. Appl. Phys.*, **78**(7), pp. 4627–4632.
- [28] Hussein, M. I., Hulbert, G. M., and Scott, R. A., 2006, "Dispersive Elastodynamics of 1D Banded Materials and Structures: Analysis," *J. Sound Vib.*, **289**(4-5), pp. 779–806.
- [29] Milton, G. W., 2002, *The Theory of Composites*, Cambridge University Press, Cambridge.
- [30] Schoenberg, M. and Sen, P. N., 1983, "Properties of a Periodically Stratified Acoustic Half-space and Its Relation to a Biot Fluid," *J. Acoust. Soc. Am.*, **73**, pp. 61–67.
- [31] Cheng, Y., Yang, F., Xu, J. Y., and Liu, X. J., 2008, "A Multilayer Structured Acoustic Cloak with Homogeneous Isotropic Materials," *Appl. Phys. Lett.*, **92**, p. 151913.
- [32] Torrent, D. and Sánchez-Dehesa, J., 2010, "Anisotropic Mass Density by Radially Periodic Fluid Structures," *Phys. Rev. Lett.*, **105**, p. 174301.
- [33] Wu, Y., Yun, L., and Zhang, Z. Q., 2007, "Effective Medium Theory for Elastic Metamaterials in Two Dimensions," *Phys. Rev. B*, **76**, p. 205313.
- [34] Zhou, X. M. and Hu, G. K., 2009, "Analytic Model of Elastic Metamaterials with Local Resonances," *Phys. Rev. B*, **79**, p. 195109.
- [35] Smith, D. R., Schultz, S., Markos, P., and Soukoulis, C. M., 2002, "Determination of Effective Permittivity and Permeability of Metamaterials from Reflection and Transmission Coefficients," *Phys. Rev. B*, **65**, p. 195104.
- [36] Chen, X. D., Grzegorzczak, T. M., Wu, B. I., Pacheco, J., and Kong, J. A., 2004, "Robust Method to Retrieve the Constitutive Effective Parameters of Metamaterials," *Phys. Rev. E*, **70**, p. 016608.
- [37] Fokin, V., Ambati, M., Sun, C., and Zhang, X., 2007, "Method for Retrieving Effective Properties of Locally Resonant Acoustic Metamaterials," *Phys. Rev. B*, **76**, p. 144302.
- [38] Popa, B. and Cummer, S. A., 2009, "Design and Characterization of Broadband Acoustic Composite Metamaterials," *Phys. Rev. B*, **80**, p. 174303.
- [39] Brekhovskikh, L., 1980, *Waves in Layered Media*, Academic, New York.
- [40] Martin, P. A., Maurel, A., and Parnell, W. J., 2010, "Estimating the Dynamic Effective Mass Density of Random Composites," *J. Acoust. Soc. Am.*, **128**, pp. 571–577.
- [41] Berryman, J. G., 1980, "Long -Wavelength Propagation in Composite Elastic Media—I. Spherical Inclusions," *J. Acoust. Soc. Am.*, **68**, pp. 1809–1819.
- [42] Berryman, J. G., 1980, "Long -Wavelength Propagation in Composite Elastic Media—II. Ellipsoidal Inclusions," *J. Acoust. Soc. Am.*, **68**, pp. 1820–1831.
- [43] Mei, J., Liu, Z. Y., Wen, W. J., and Sheng, P., 2006, "Effective Mass Density of Fluid-Solid Composites," *Phys. Rev. Lett.*, **96**, p. 024301.
- [44] Torrent, D. and Sánchez-Dehesa, J., 2006, "Effective Parameters of Clusters of Cylinders Embedded in a Nonviscous Fluid or Gas," *Phys. Rev. B*, **74**, p. 224305.
- [45] Huang, H. H. and Sun, C. T., 2009, "Wave Attenuation Mechanism in an Acoustic Metamaterial with Negative Effective Mass Density," *New J. Phys.*, **11**, p. 013003.